The IDA3 adapter, required for intraflagellar transport of I1 dynein, is regulated by ciliary length

Emily L. Hunter[a], Karl Lechtreck[b], Gang Fu[c], Juyeon Hwang[a], Huawen Lin[d], Avanti Gokhale[a], Lea M. Alford[e], Brian Lewis[d], Ryosuke Yamamoto[f], Ritsu Kamiya[g], Fan Yang[h], Daniela Nicastro[c], Susan K. Dutcher[d], Maureen Wirschell[h], and Winfield S. Sale[a,*]

[a]Department of Cell Biology, Emory University, Atlanta, GA 30322; [b]Department of Cellular Biology, University of Georgia, Athens, GA 30602; [c]Departments of Cell Biology and Biophysics, University of Texas Southwestern Medical Center, Dallas, TX 75390; [d]Department of Genetics, Washington University School of Medicine, St. Louis, MO 63110; [e]Department of Biology, Oglethorpe University, Atlanta, GA 30319; [f]Department of Biological Sciences, Osaka University, Osaka 560-0043, Japan; [g]Department of Biological Sciences, Chuo University, Tokyo 112-8551, Japan; [h]Department of Biochemistry, University of Mississippi Medical Center, Jackson, MS 39216

ABSTRACT **Axonemal dyneins, including inner dynein arm I1, assemble in the cytoplasm prior to transport into cilia by intraflagellar transport (IFT). How I1 dynein interacts with IFT is not understood. We take advantage of the *Chlamydomonas reinhardtii ida3* mutant, which assembles the inner arm I1 dynein complex in the cytoplasm but fails to transport I1 into the cilium, resulting in I1 dynein-deficient axonemes with abnormal motility. The *IDA3* gene encodes an ~115-kDa coiled-coil protein that primarily enters the cilium during ciliary growth but is not an axonemal protein. During growth, IDA3, along with I1 dynein, is transported by anterograde IFT to the tip of the cilium. At the tip, IDA3 uncouples from IFT and diffuses within the cilium. IFT transport of IDA3 decreases as cilia lengthen and subsides once full length is achieved. IDA3 is the first example of an essential and selective IFT adapter that is regulated by ciliary length.**

Monitoring Editor
Erika Holzbaur
University of Pennsylvania

Received: Dec 20, 2017
Revised: Feb 9, 2018
Accepted: Feb 16, 2018

INTRODUCTION

Cilia, also known as flagella, play essential roles in motility and cell signaling (Ostrowski *et al.*, 2011; Viswanadha *et al.*, 2017). Defective ciliary motility results in human disease, including primary cilia dyskinesia (PCD) (Horani *et al.*, 2016; Knowles *et al.*, 2016). Defective motility can arise from the failure to assemble dynein arms (Kamiya and Yagi, 2014). Proper assembly of axonemal dynein arms requires not only the structural components, such as dynein heavy, intermediate, and light chains, but also factors extrinsic to the dynein for cytoplasmic assembly (Iomini *et al.*, 2009; Kobayashi and Takeda, 2012), intraflagellar transport (IFT) (Hou *et al.*, 2007; Ahmed *et al.*, 2008; Viswanadha *et al.*, 2014; Desai *et al.*, 2015; Lechtreck, 2015; Hou and Witman, 2017; Taschner *et al.*, 2017), and docking in the axoneme (Owa *et al.*, 2014; Brown *et al.*, 2017). We are only beginning to understand the key proteins and mechanisms required to assemble and transport ciliary dyneins, as well as other complexes in the axoneme (Lechtreck *et al.*, 2017).

Here we focus on the IFT transport of the inner dynein arm I1/f (Kamiya and Yagi, 2014; King, 2016). I1 dynein is assembled into a large 20S complex in the cytoplasm that is transported by IFT to the tip of the cilium for assembly in the axoneme (Viswanadha *et al.*, 2014). How I1 interacts with IFT remains unknown. While tubulin binds IFT directly through IFT81/IFT74 (Bhogaraju *et al.*, 2014; Craft *et al.*, 2015; Kubo *et al.*, 2016; Taschner *et al.*, 2016; Hou and Witman, 2017), the outer dynein arm (ODA) requires the specialized adapter protein ODA16 to interact with IFT46 for efficient transport (Ahmed *et al.*, 2008; Hou and Witman, 2017; Taschner *et al.*, 2017). Whether I1 or other inner dynein arms require specialized adapters to bind IFT remains unknown.

Through study of the *Chlamydomonas* I1 dynein mutant *ida3*, we show that the IDA3 protein is a specialized and transient IFT adapter required to load I1 dynein onto IFT for entry and transport in the

This article was published online ahead of print in MBoC in Press (http://www.molbiolcell.org/cgi/doi/10.1091/mbc.E17-12-0729) on February 19, 2018.
The authors declare no competing financial interests.

*Address correspondence to: Winfield S. Sale (wsale@emory.edu).

Abbreviations used: DTT, dithiothreitol; IFT, intraflagellar transport; NG, NeonGreen.

growing cilium. Unlike the loading and transport of ODA16, which binds IFT regardless of cilium length (Ahmed *et al.*, 2008), IDA3 loading and transport are regulated by changes in cilium length in a cilium autonomous manner, similar to the axonemal cargoes such as tubulin (Craft *et al.*, 2015). Thus, IDA3 is unique in that it behaves similarly to an axonemal cargo of IFT, but neither binds the axoneme nor remains in the cilium once full length is achieved. We suggest that other axonemal complexes also require specialized and transient IFT adapters to precisely control entry and transport in the cilium.

RESULTS AND DISCUSSION

Inner dynein arm I1 is specifically missing in *ida3* mutant axonemes

Although the 20S I1 complex forms in the *ida3* cytoplasm, I1 dynein does not enter the cilium, preventing I1 incorporation into the axoneme (Kamiya *et al.*, 1991; Viswanadha *et al.*, 2014). We examined the structure of the *ida3* axoneme by cryo–electron tomography and subtomogram averaging. Tomographic slices (Figure 1A, a–f) and isosurface renderings (Figure 1A, g–j) reveal that I1 dynein is missing in *ida3* axonemes, except on rare occasions (Supplemental Figure S1A, a–e). Notably, all other axonemal structures assemble properly in the *ida3* axoneme, as also seen by thin-section electron microscopy (Supplemental Figure S1B). Thus, like other I1 dynein mutants that include *ida1, ida2, ida7,* and *bop5* (Wirschell *et al.*, 2007; Heuser *et al.*, 2012; Ishikawa, 2012; Kamiya and Yagi, 2014; King, 2016), only I1 dynein fails to assemble in *ida3* axonemes. In contrast to other I1 mutants, all known I1 dynein subunits of the 20S I1 dynein complex assemble in the *ida3* cytoplasm (Viswanadha *et al.*, 2014). We postulated that *IDA3* encodes a protein extrinsic to I1 dynein that is specifically required for ciliary entry and/or transport of I1 dynein by IFT.

A nonsense mutation in *IDA3* results in loss of I1 dynein in the axoneme

The *ida3* mutant was mapped to a small region on Chromosome 3 between markers 953 and 120055. This 369-kb region contains the centromere, and better resolution could not be obtained with additional markers. With 40× coverage of the *ida3* genome, we identified only one SNP in the mapped region after filtering. This change is in Cre03.g205000, and there is a G-to-A transition that changes a tryptophan codon (TGG) to a stop codon (TAG) at amino acid 22 (Figure 1B; Supplemental Figure S2 Table I). This mutation cosegregates with the slow-swimming phenotype in 75 meiotic progeny. Transformation of *ida3* with an untagged *IDA3* or *IDA3* fused to 3xHA or NeonGreen (NG) rescued I1 assembly in the axoneme and the slow-swimming phenotype (Figure 1, C and D; Supplemental Figures S1B and S2 Table II). Reversion (Lin and Dutcher, 2015) of *ida3* in the *ida3; oda2* double mutant (defective in I1 and outer dynein arm assembly) rescues assembly of I1 dynein in the axoneme and paralysis of *ida3; oda2* (Figure 1E; Supplemental Figure S2 Table III). Together, these data confirm that Cre03.g205000 *(IDA3)* is the defective gene in *ida3*.

IDA3 is transported by anterograde IFT within the regenerating cilium

The *IDA3* gene encodes an ~115-kD coiled-coil protein that contains a CCDC24 domain (Pfam domain PF15669) in the N-terminal quarter of the protein (indicated by the bar, Figure 1B; Supplemental Figure S2, A and B), whereas the C-terminal half of IDA3 does not show conservation outside of green algae. Immunoblot analysis of cytoplasmic extract from *ida3; IDA3::HA* revealed that IDA3::HA is present in the cytoplasm of ciliated cells but not in axonemes (Figure 1, F and G).

Given the 20S I1 dynein does not enter the cilium in *ida3* (Viswanadha *et al.*, 2014), we predicted that IDA3 function would be tightly linked to I1 dynein transport into the cilium. To test this prediction, we analyzed matrix (soluble fraction of isolated cilia) (Cole *et al.*, 1998; Craige *et al.*, 2013) from full-length and regenerating *ida3; IDA3::HA* cilia. IDA3::HA, though absent in the matrix of full-length cilia, is present in the matrix of regenerating cilia, as are the intermediate chains IC140 and IC138 of I1 dynein (Figure 2, A and B). Thus, I1 only enters the cilium when IDA3 is present. Together, these data demonstrate that IDA3, though not an axonemal component, selectively enters cilia during regeneration and is essential for I1 entry into the cilium. IDA3 appears to be modified in the matrix of regenerating cilia, as indicated by the presence of two distinct IDA3 bands (arrowheads, Figure 2B). The nature of this modification remains unknown.

I1 dynein, marked by IC140::GFP, is transported by anterograde IFT (Supplemental Figure S3A). Given that IDA3 is essential for I1 assembly in the axoneme, we asked if IDA3 is also a cargo of IFT inside the cilium. Using live-cell total internal reflection fluorescence microscopy (TIRF) (Lechtreck, 2013), we imaged *ida3; IDA3::NG* cells with either full-length or regenerating cilia (Supplemental Movie 1). Similarly to bona fide axonemal proteins (Lechtreck *et al.*, 2017), IFT transport of IDA3::NG in regenerating cilia is robust, whereas IDA3 transport in full-length cilia is rare (Figure 2, C and D). Approximately 90% of individual IDA3::NG particles are transported processively to the distal tip of the cilium at a velocity of 1.98 ± 0.37 µm/s, consistent with the speed of anterograde IFT in *Chlamydomonas* (Figure 2, Ea–G; Supplemental Figure S3, B–D). Occasionally, we observed stationary IDA3::NG (Figure 2Ed). This could result from stalling of IFT trains along the length of the axoneme, as recently described (Stepanek and Pigino, 2016), or by transient association with the axoneme. At the tip, multiple IDA3 proteins linger before diffusion begins (Supplemental Figure S3, B and C, white arrows). IDA3::NG then diffuses within the cilium ~ 88% of the time (Figure 2, Ec and H). Occasionally, retrograde IFT transports IDA3::NG at a velocity of 2.66 ± 1.2 µm/s (Figure 2, E(b) and H; Supplemental Figure S3D). One possibility is that diffusion of IDA3 through the cilium into the cell body controls the pool of IDA3 available for I1 transport (Chien *et al.*, 2017; Wingfield *et al.*, 2017).

IDA3 transport by anterograde IFT is dependent on ciliary length

To further explore the link between IDA3 and ciliary growth, we quantified the number of IDA3::NG particles that enter the cilium as it lengthens. Similarly to axonemal cargoes of IFT (Wren *et al.*, 2013; Craft *et al.*, 2015), the number of IDA3 particles transported per minute decreases as the cilium lengthens (Figure 3A). Thus, IDA3 is the first identified nonaxonemal cargo of IFT whose transport frequency is regulated by ciliary length. It is possible that the transport of IDA3, in addition to axonemal cargoes of IFT, may be regulated by mechanisms that control cilium length (Chien *et al.*, 2017; Ishikawa and Marshall, 2017). The quantity of cargo transported by IFT at any given time may also be regulated by ciliary length.

We next asked whether IDA3 would selectively enter the growing cilium in a cell that had one growing and one full-length cilium. *ida3; IDA3::NG* cells with one regenerating (short) cilium and one full-length (long) cilium were imaged by TIRF (Supplemental Movie S2; Craft *et al.*, 2015). Anterograde IFT transport, dwell at the tip of the cilium, and diffusion of IDA3::NG were observed only in the regenerating cilium (Figure 3, B and C). These data confirm that

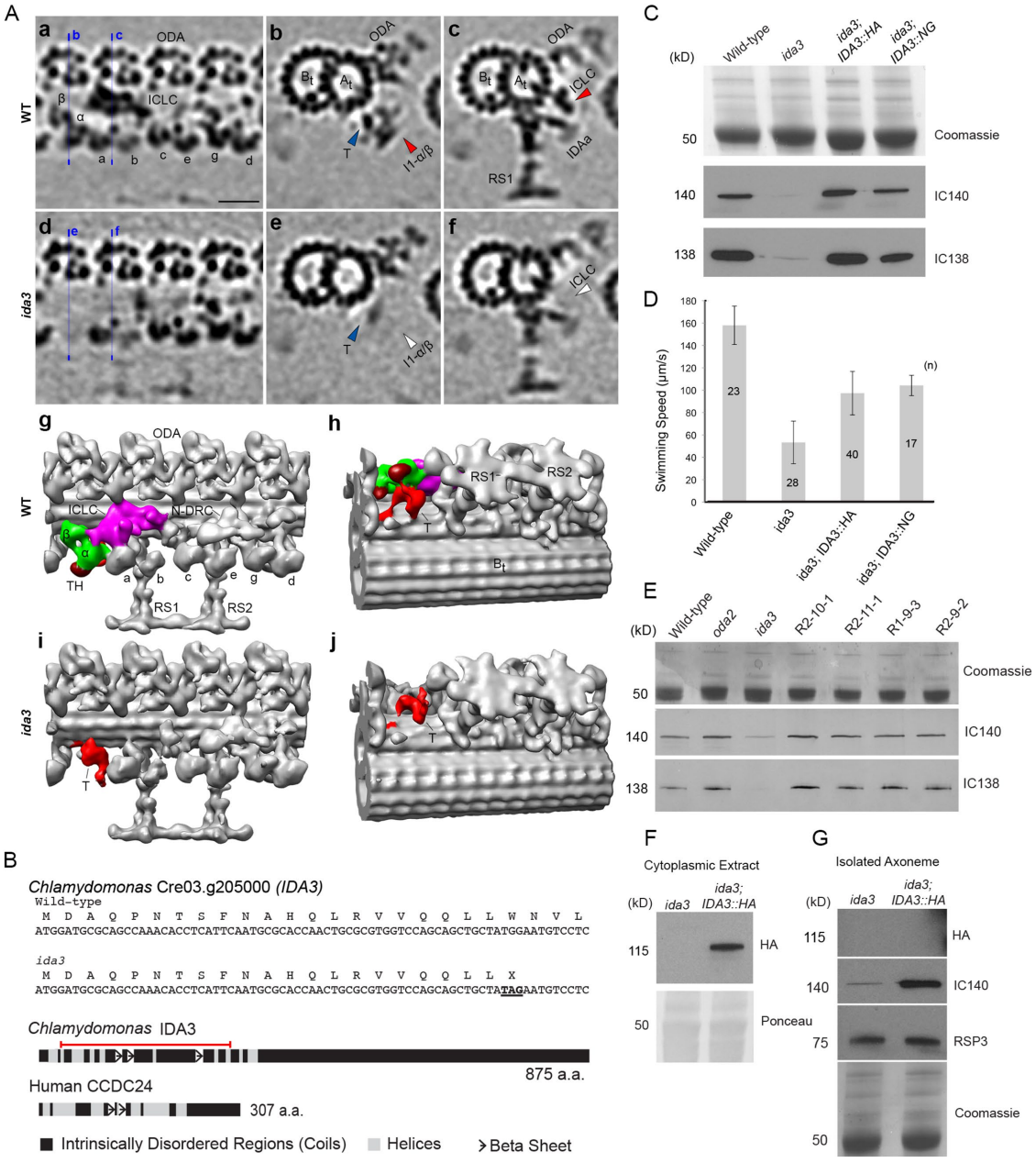

FIGURE 1: I1 dynein is specifically missing in *ida3* axonemes and Cre03.g205000 *(IDA3)* rescues *ida3* I1 dynein defect. (A) Cryo-EM images of tomographic slices show the averaged axonemal 96-nm repeats from WT (a–c) and *ida3* mutant (d–f) in longitudinal (a, d) and cross-sectional (b, c, e, f) views. The localization of cross-sectional slices at I1 dynein heads (red arrowhead in b and white arrowhead in e) or intermediate chain/light chain complex (ICLC) (red arrowhead in c and white arrowhead in f) is indicated by the blue lines in a and d. 3D isosurface renderings show the front (g, i) and rotated bottom (h, j) views. The I1-tether structure (T) (blue arrowheads in b and e and red structures in g–j) is still visible in *ida3* (i, j), but the position and morphology differ somewhat from WT, likely due to the absence of the tether binding partners, the I1 dynein heads. The WT data have been published previously (Awata *et al.*, 2015). Scale bar: 20 nm. (B) In the *ida3* mutant, Cre03.g205000 contains a nonsense mutation. IDA3 contains a CCDC24 domain (red bar) in the N-terminal half. (C) Immunoblot of isolated axonemes from WT, *ida3, ida3;IDA3::HA,* and::*NG* cells probed with antibodies to IC140 and IC138. (D) Swimming speed analysis for wild type (CC-125), *ida3, ida3; IDA3::HA,* and::*NG. ida3* slow swimming phenotype is rescued in *ida3* transformants. Error bars = SD. (E) Immunoblot of axonemes from *ida3; oda2* intragenic revertants. IC140 and IC138 assemble in axonemes from the intragenic revertants. (F) Immunoblot of cytoplasmic extract isolated from fully ciliated *ida3* and *ida3; IDA3::HA* cells. IDA3::HA is detected in the cytoplasm. (G) Immunoblot of axonemes from *ida3* and *ida3; IDA3::HA* full-length cilia. IDA3::HA is not present in the axonemes, but IC140 assembles as expected.

IDA3 selectively enters the growing cilium and indicate that transport of the IDA3 is regulated independently within each of the two cilia in a single *Chlamydomonas* cell. This behavior is reminiscent of the regulation of tubulin–IFT interaction (Craft *et al.*, 2015). How the cell selectively targets IDA3 into the growing cilium remains unknown.

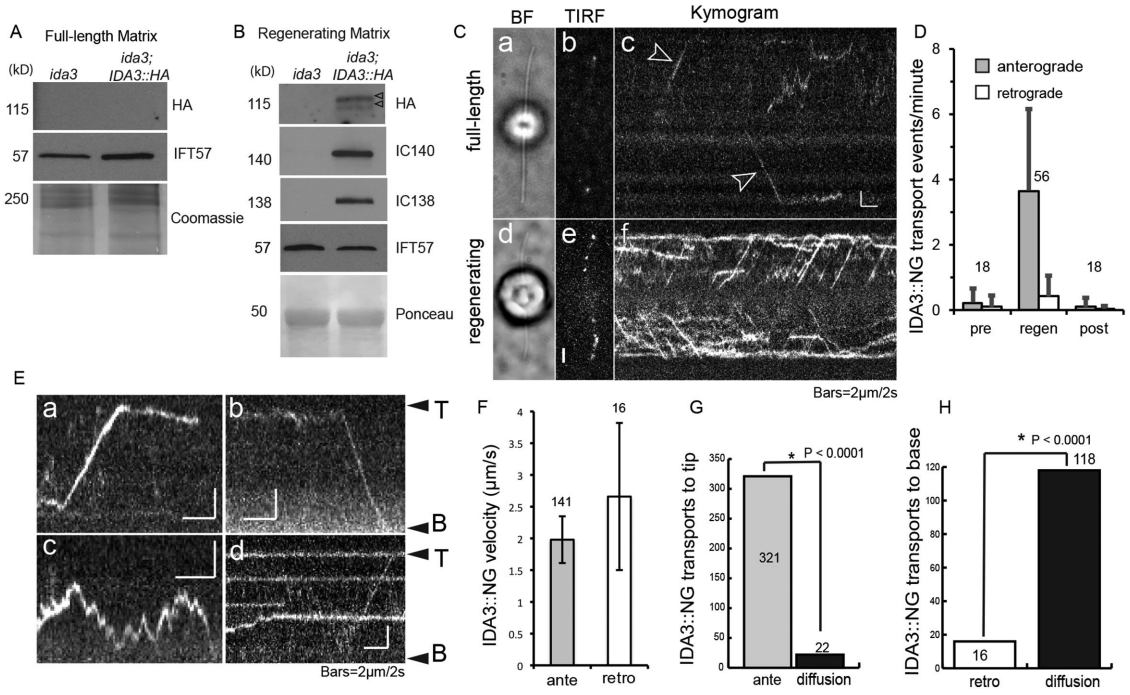

FIGURE 2: IDA3 is transported by anterograde IFT in regenerating cilia. (A) Immunoblot of matrix from *ida3* and *ida3; IDA3::HA* full-length cilia. Immunoblots were probed with antibodies to HA, and as a loading control, IFT57. IDA3::HA was not detectable in the matrix of full-length *ida3; IDA3::HA* cilia. (B) Immunoblot of matrix isolated from *ida3* and *ida3; IDA3::HA* regenerating cilia. Immunoblots were probed with antibodies to HA, IC140, IC138, and, as a loading control, IFT57. IDA3::HA, IC140, and IC138 are present in the regenerating matrix of *ida3; IDA3::HA*. (C) Bright field (a, d) and TIRF images (b, e) and corresponding kymograms (c, f) of full-length (a–c) and regenerating (d–f) *ida3; IDA3::NG* cilia. Selected IDA3::NG transports are marked with arrowheads in c. Bars = 2 s and 2 μm. (D) Bar diagram showing the frequency of IDA3::NG transport events per minute in full-length (pre; $n = 18$ cilia), regenerating (regen; $n = 56$ cilia), and postregeneration cilia (post; $n = 18$ cilia ~10–12 μm in length). Error bars = SD. (E) Kymograms of IDA3::NG transport in regenerating cilia. (a) Anterograde transport of IDA3::NG, (b) retrograde transport of IDA3::NG, (c) diffusion of IDA3::NG throughout the cilium, (d) stationary IDA3::NG. Bars = 2 s and 2 μm; T: tip, B: base. (F) Velocity of IDA3::NG transport in the cilium. Processive anterograde IDA3::NG moves at a velocity of 1.98 μm/s ($n = 141$). Retrograde IDA3::NG transport moves at 2.66 μm/s ($n = 16$). Error bars = SD. (G) Number of IDA3::NG anterograde IFT vs. diffusion events from base to tip. Two-tailed binomial test reveals a significant difference in the quantity of IDA3::NG anterograde transport events compared with diffusion ($P < 0.0001$). (H) Quantity of IDA3::NG retrograde IFT transport vs. diffusion. IDA3::NG seldom binds retrograde IFT ($n = 16$) and instead diffuses through the cilium ($n = 118$). Two-tailed binomial test reveals a significant difference in IDA3::NG retrograde transport events compared with diffusion ($P < 0.0001$).

Given the specificity of IDA3 for I1 dynein, we predicted that the need to assemble I1 dynein in the axoneme prompts IDA3 entry/transport in the growing cilium. To test this, we mated *ida3* x *ida3; IDA3::NG* to generate dikaryons with four cilia: two full-length cilia with I1 docked in the axoneme and two full-length cilia lacking I1 dynein (Figure 3D). TIRF imaging revealed that IDA3::NG rarely enters any of the four cilia, consistent with the infrequent transport of IDA3 in full-length cilia (Figure 3E). Hence, it is changes in ciliary length, and not the need to assemble I1 dynein in the axoneme, that cue increased IDA3 transport. However, infrequent transport of IDA3 and I1 is eventually sufficient to rescue I1 dynein assembly and motility in the full-length axoneme (Viswanadha *et al.*, 2014).

Stable binding of IDA3 to IFT requires I1 dynein

We investigated whether IDA3 transport by IFT also requires I1 dynein. We isolated the triple mutant *ida7*; *ida3*; *IDA3::NG*, which carries a mutation in the *IC140* gene (Perrone *et al.*, 1998) that prevents cytoplasmic assembly of the 20S I1 dynein (Viswanadha *et al.*, 2014), but carries wild-type IDA3::NG. IDA3::NG is expressed and is stable in this *ida7* background (see Viswanadha *et al.*, 2014). TIRF imaging revealed that IDA3::NG is transported by IFT in growing cilia even in the absence of I1 dynein (Figure 4, A–C; Supplemental Movie S3). However, in the wild type, IDA3 is typically transported without interruption from the base to the ciliary tip, whereas in the absence of I1, IDA3::NG transport is less processive (Figure 4D; Supplemental Movie S3). For example, in wild-type cilia, 74% of the transports are processive from base to tip, whereas, in the *ida7* background, only 30% of transport is continuous from base to tip ($n = 80$ and 61 transports, respectively). As a consequence of increased dissociation of IDA3 from IFT, IDA3::NG diffusion is prominent in growing *ida7*; *ida3*; IDA3::NG cilia (Figure 4A). Thus, IDA3 is transported by IFT in the absence of I1, but the IDA3–IFT interaction appears to be more transient, suggesting that I1 dynein stabilizes the IDA3–IFT interaction. Given that I1 dynein does not bind IFT in the absence of IDA3, we suggest that IDA3 bound to IFT renders IFT competent to bind and transport I1 dynein. In turn, I1 dynein possibly stabilizes IDA3 interaction with IFT.

IDA3 interacts biochemically with IC140 in the matrix of regenerating cilia

Considering that IDA3 permits entry/transport of I1 dynein in the cilium, we predicted that IDA3 and I1 dynein interact while in transit

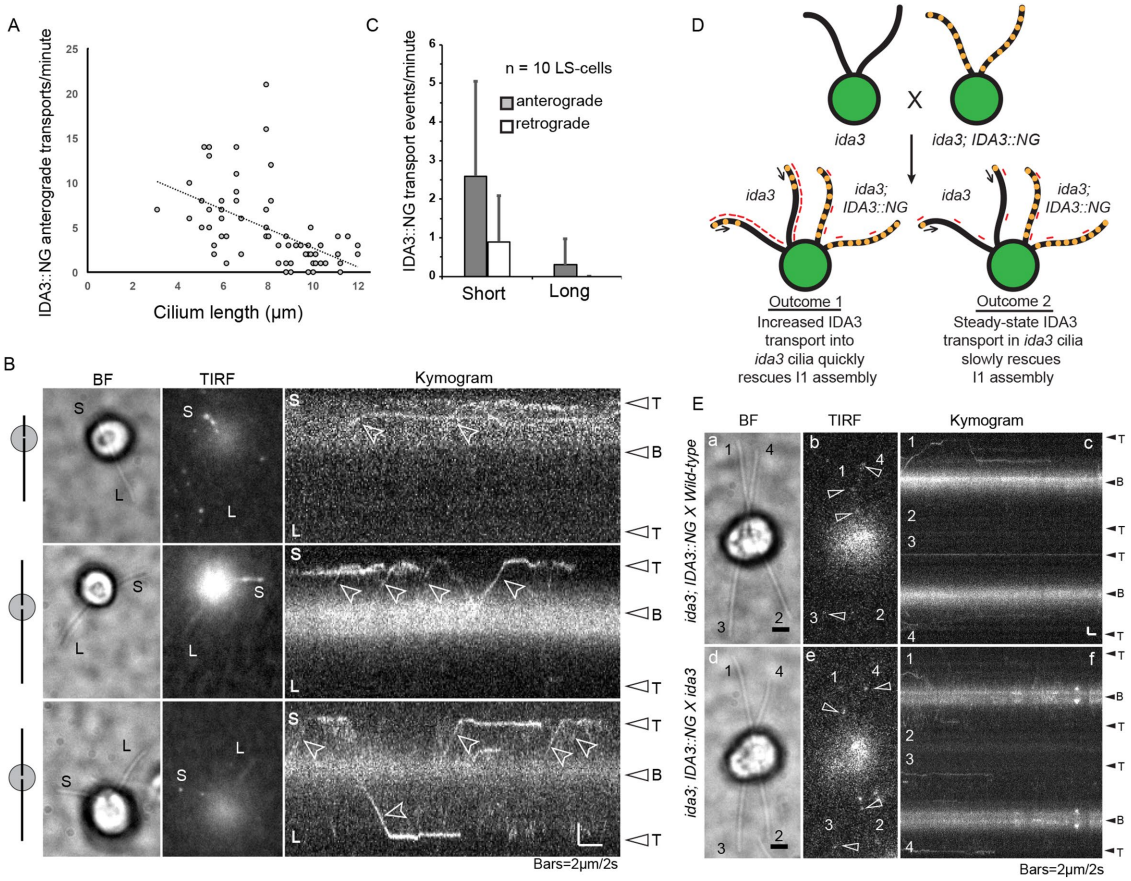

FIGURE 3: IDA3 transport by anterograde IFT is regulated by ciliary length. (A) The frequency of IDA3::NG anterograde transport events compared with cilium length. As the length of the cilium increases, the quantity of IDA3::NG transported by anterograde IFT decreases. (B) Still frames and kymograms of IDA3::NG transport in *ida3; IDA3::NG* cilia of long-short (LS) cells. Frequent anterograde IFT transport of IDA3::NG only occurs in the regenerating cilium (open arrowheads). Bar = 2 s and 2 μm (C) Quantification of IDA3::NG transport frequency in the short and long cilia of LS cells ($n = 10$ cells). Error bars = SD. (D) Schematic representation of dikaryon rescue experiment that results in *ida3 x ida3; IDA3::NG* zygotes. Orange dots indicate I1 docked in axoneme. Red dashes indicated IDA3 transport by IFT. (E) Bright field (a, d), TIRF images (b, e), and corresponding kymograms (c, f) of *ida3; IDA3::NG* × wild-type dikaryon (a–c) and *ida3; IDA3::NG* × *ida3* dikaryons (d–f). IDA3::NG transport is rare in all four full-length cilia, regardless of I1 absence in the axoneme. Bar = 2 s and 2 μm.

to the ciliary tip. Immunoprecipitation of IDA3::HA from the matrix of regenerating *ida3; IDA3::HA* cilia revealed the presence of both IDA3::HA and IC140 in pull down (Figure 5A). IDA3::HA was also detected in complementary pull downs of IC140::SNAP from the regenerating matrix of the quadruple mutant *ida7; IC140::SNAP; ida3; IDA3::HA* cilia (Figure 5B). Together these data suggest co-transport of IDA3 and I1 dynein to the tip of the growing cilium (Figure 5C). While a modified form of IDA3::HA exists in the matrix of regenerating cilia (Figure 2B), only one of the two bands is pulled down in our interaction studies (Figure 5, A and B). Whether the IDA3 modification regulates IDA3-I1 dynein interaction remains to be determined.

Summary and conclusions

IFT adapters are defined as proteins present on IFT machinery that are not integral to the overall assembly and function of IFT. To date, ODA16, required for efficient transport of ODA, is one of the best-described IFT adapters (Ahmed *et al.*, 2008; Hou and Witman, 2017; Taschner *et al.*, 2017). Although both ODA16 and IDA3 are needed to assemble specific axonemal components, IDA3 predominantly binds IFT during ciliary assembly, while ODA16 binds IFT regardless of cilium length (Ahmed *et al.*, 2008). Thus, ODA16 behaves as an IFT component, while IDA3 behaves as a cilium length–dependent cargo of IFT. Considering the contrast in IDA3 and ODA16 behavior, it may be necessary to redefine the in vivo properties that define an adapter to IFT as compared with a genuine IFT component. Predictably, other large axonemal components (other inner dynein arms, the radial spokes, or N-DRC) may require their own highly specialized and transient adapters to attach to IFT.

IFT transport of I1 dynein is dependent on the adapter IDA3, and in the absence of IDA3, I1 fails to enter the cilium. The requirement for IFT-mediated I1 dynein entry supports the notion that axonemal components destined to enter the cilium do so based on their ability to bind IFT. Analogously to adapters for cytoplasmic dynein–cargo interaction (e.g., Redwine *et al.*, 2017), adapters may play an essential role in allowing the ~22 IFT core proteins to bind hundreds of different axonemal proteins and protein complexes (Taschner and Lorentzen, 2016; Lechtreck *et al.*, 2017). IDA3 is highly specific for I1 dynein (Figure 1A; Supplemental Figure S1B). Thus, highly specialized adapters, such as IDA3, may be the key to regulating IFT loading and to precisely adjusting the quantity of individual cargoes

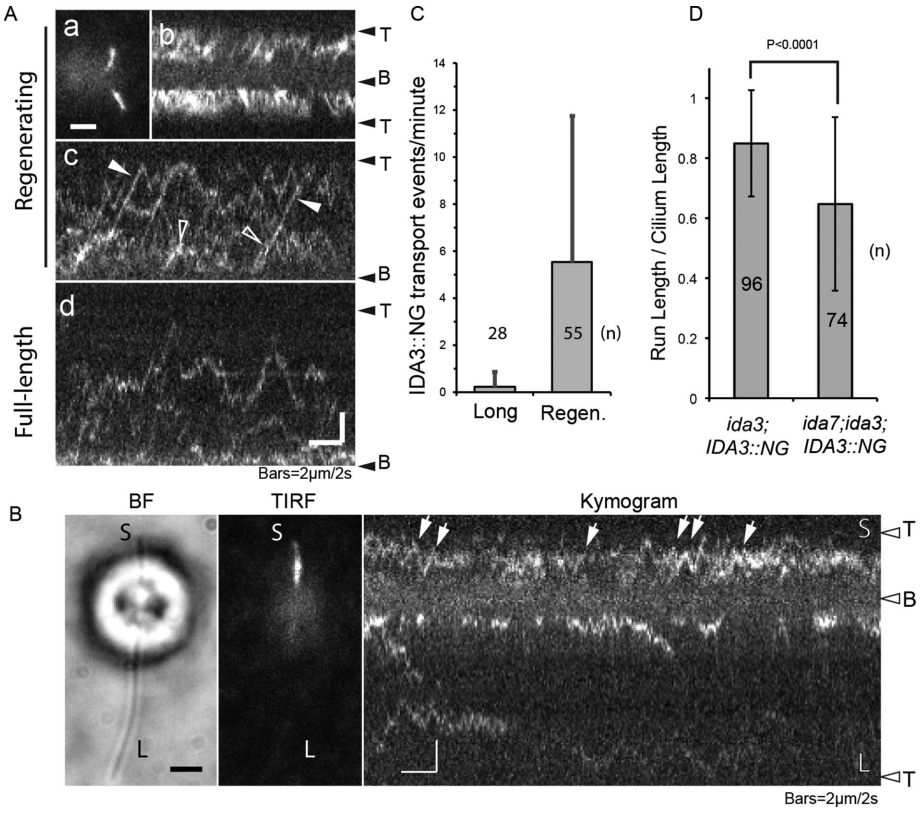

FIGURE 4: Efficient IFT transport of IDA3 requires I1 dynein. (A) *ida7; ida3; IDA3::NG* cells, lacking I1 dynein, imaged by TIRF. (a) Still frame of regenerating *ida7; ida3; IDA3::NG* cilia and (b, c) kymograms of IDA3::NG transport in regenerating *ida7; ida3; IDA3::NG* cilia. IDA3::NG both undergoes anterograde IFT (white arrowheads) and diffuses (open arrowheads) in the absence of I1 dynein. (d) Kymogram of IDA3::NG diffusion in full-length *ida7; ida3; IDA3::NG* cilia. IDA3::NG processive motion is rarely observed. Bars = 2 s and 2 μm. (B) Still frames and kymogram of an *ida7; ida3; IDA3::NG* short–long cell. IDA3::NG transport is restricted to regenerating cilium. Bar = 2 s and 2 μm. (C) Quantification of IDA3::NG transport events per minute in long and regenerating *ida7; ida3; IDA3::NG* cilia. Error bars = SD. (D) Analysis of IDA3 transport efficiency in the presence and absence of I1. The lengths of IDA3::NG anterograde IFT tracks were compared with the length of the cilium in *ida3; IDA3::NG* ($n = 96$) and *ida7; ida3; IDA3::NG* ($n = 74$) cilia. IDA3::NG transport is less processive in the absence of I1. A two-tailed unpaired *t* test confirms a significant difference in the length of anterograde IFT tracks in *ida3; IDA3::NG* and *ida7; ida3; IDA3::NG* cells ($P < 0.0001$). Error bars = SD.

transported into the cilium at any given time. IDA3 attachment to IFT, like axonemal cargoes of IFT but unlike IFT proteins, responds to changes in cilium length. Further study will be required to determine how IDA3 loading and transport are regulated by changes in cilium length.

MATERIALS AND METHODS

Strains and culture conditions

C. reinhardtii strains used include wild type (CC-124, CC-125, CC-620, CC-621), *ida3* (CC-2668), *ida3; oda2*, *ida7* (CC-3921), *ida3; IDA3::HA*, *ida3; IDA3::NG*, *ida7; ida3; IDA3::NG*, *ida3; IDA3::HA; ida7; IC140::SNAP*, *ida7; IC140::GFP*, *oda6; ida7; IC140::GFP*, and the polymorphic strain CC-1952 (S1C5). Cells were cultured in either tris-acetate-phosphate (TAP) medium, L medium, or M medium (Harris, 2009) with aeration on a 14:10 h light/dark cycle or under constant light. Wild type, *ida7*, CC-1952 (S1C5), and *ida3* were acquired through the Chlamydomonas Resource Center (University of Minnesota). All other strains were generated specifically for this publication.

Generation of ida7; IC140::SNAP

A GFP-tagged IC140 construct, containing the *APHVIII* selection cassette (Sizova *et al.*, 1996), was generated from clone pCP3 (Perrone *et al.*, 1998). The *APHVIII* cassette was inserted into pCP3 with *Sma*I and *Kpn*I to produce the plasmid *IC140::GFP-AphVIII*. The 3.28-kb *Nru*I–*Eco*RI fragment from *IC140::GFP-APHVIII* was excised and subcloned into plasmid pSE280 to produce pCS5.1. A 2.068-kb *Nru*I-*Rsr*II fragment containing the SNAP tag in place of GFP in exon 2 was synthesized and cloned into the pUC57-Kan vector (Genscript) to make clone pCS17. The *Nru*I-*Rsr*II fragment from pCS17 was excised and subcloned into the pCS5.1 plasmid to produce pCS18. A 2.71-kb *Psp*XI-*Eco*RV fragment from pCS18 was subcloned into the *IC140::GFP-AphVIII* clone to produce pCS20, which contains the *IC140* gene fused to SNAP in exon 2. Plasmid pCS20 was used to transform the *ida7* strain using the glass bead method (Kindle, 1990). Paromomycin-resistant colonies were selected and examined for assembly of the SNAP::IC140 fusion protein in axonemes and for motility. Several transformants were selected that displayed wild type–like motility.

Generation of oda6; ida7; IC140::GFP

To visualize the IC140 movement in cilia, a rescued strain of *oda6; ida7* expressing exogenous IC140::GFP molecules was generated (*oda6; ida7R::GFP*) and used for the TIRF analyses. To generate the *oda6; ida7R::GFP* strain, *oda6; ida7* mutants were transformed with the vector *pCP3-GFP-APHVIII*, which had the pBlueScript backbone and contained an *Xba*I-*Sma*I *Chlamydomonas* genomic fragment covering all the IC140 genomic region with a GFP inserted in either the first or second exon of the IC140 gene. *pCP3-GFP-APHVIII* also had the *APHVIII*-gene cassette, which confers paromomycin resistance to transformants. Transformation was carried out by the electroporation method with successful rescue of *ida7* with either the GFP DNA tag in exon 1 (pCP3-GFP(E1)-AphVIII) or 2 (pCP3-GFP(E2)-AphVIII) of the IC140 gene. For TIRF microscopy we used IC140 with the GFP inserted in exon 1. We also used TIRF microscopy to observe I1 dynein transport analyzed *ida7;* IC140::GFP obtained from Oda *et al.* (2015).

Constructing double, triple, and quadruple mutants

Strains (e.g., *ida3;oda2*, *ida7; ida3::IDA3-NG*, and *ida3; IDA3::HA; ida7; IC140::SNAP*) were crossed by standard protocols (Dutcher, 1995). To generate the *ida3; oda2* mutant, cells were treated with dbcAMP and IBMX (Pasquale and Goodenough, 1987) for 30 min to allow mating of a strain with short or no flagella. Markers were determined by PCR with the following primers: *ida7* via pMN24 sequences (AAT ACG CAA ACC GCC TCT C and TGG CGT AAT CAT GGT CAT AGC), IDA3::HA (ATC GAT CCG GAC GAC CGT ACC C and GTG GTG ACG TAG TCC AGC AG), and IC140::SNAP via the

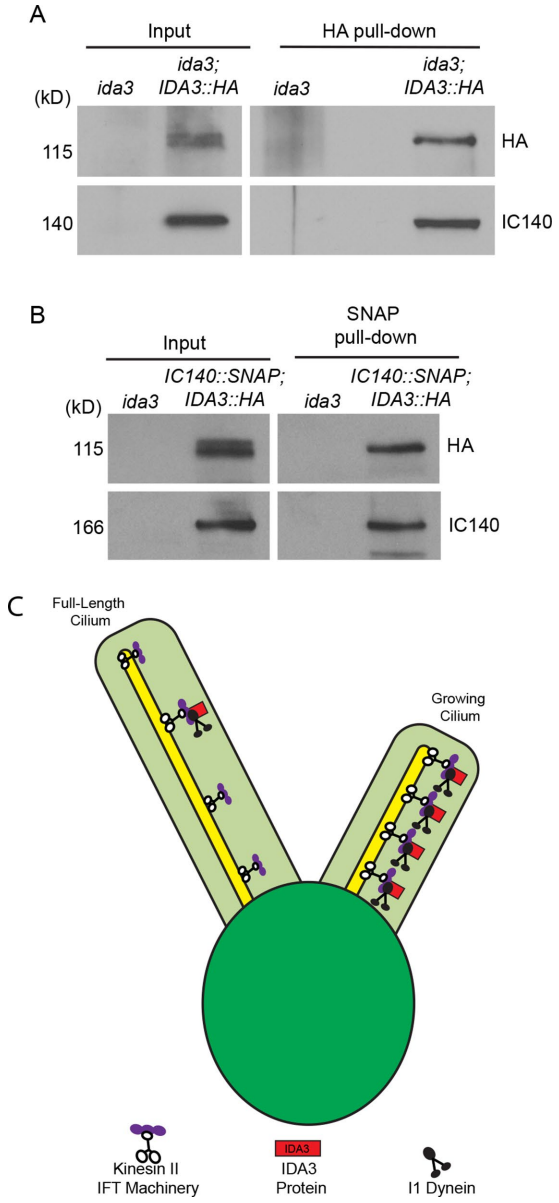

FIGURE 5: IDA3 interacts with IC140 of the I1 dynein complex in the matrix of the regenerating cilium. (A) IDA3::HA was immunoprecipitated from matrix of regenerating cilia from *ida3; IDA3::HA*. Both IDA3::HA and IC140 were detected in the IP fraction. (B) IC140::SNAP pull downs from matrix of regenerating *ida3* and *ida3; IDA3::HA; ida7; IC140::SNAP* cilia. Both IC140::SNAP and IDA3::HA were detected in SNAP pull-down samples. IC140 runs at 166 kD due to the addition of SNAP. (C) Model of cilium autonomous IDA3 behavior and function in growing cilia (adapted from Viswanadha *et al.*, 2014; Craft *et al.*, 2015). In the full-length cilium, transport of IDA3 by anterograde IFT is rare. In growing cilia, IDA3 transport by anterograde IFT increases, permitting transport of I1 dynein to the distal tip of the cilium. As the cilium elongates, the frequency of IDA3 transport events decreases. IDA3 attachment to IFT likely modifies IFT in a way that renders IFT competent to carry I1 dynein.

SNAP tag (ATC AAG CTG CTG GGC AA and GAT CAC CTC GCC CAA CTT). Loss of I1 dynein, indicative of the *ida7* mutation, was confirmed by immunoblot analysis of isolated axonemes.

Dikaryons between *ida3* and *ida3; IDA3::NG* were generated by differentiating each cell type for 6–16 h in M-N/5 medium prior to mixing the gametes of each cell type (Harris, 2009), and the zygotes with full-length, steady-state cilia were observed by TIRF microscopy.

Molecular mapping and whole-genome sequencing

Strain CC-2668 (*ida3*) was backcrossed to wild-type cells (CC-125) five times.

The backcrossed *ida3* strain was crossed to CC-1952 (S1C5) and 230 progeny were used in mapping. Crude DNA preparation, PCR, and enzymatic digestion of DNA from individual progeny were performed as previously described (Lin and Dutcher, 2015). The single *ida3* progeny was subjected to whole genome sequencing (Lin *et al.*, 2013; Lin and Dutcher, 2015). The NCBI accession number for the raw sequencing reads of *ida3* is SRX525037. We had 40x coverage of the *Chlamydomonas* genome (Lin *et al.*, 2013). The *ida3* nonsense mutation was confirmed in both *ida3* and *ida3; oda2* by PCR (Primers: ACT TGC TTT CTC ACG GCA CT and CCA TGA GAC TCC TTC CGT GT) and Sanger sequencing.

Reversion analysis

UV light at 750 µJ was used to mutagenize *ida3; oda2* (Lin and Dutcher, 2015). UV-mutagenized *ida3; oda2* plates were incubated in the dark overnight. After 1–2 d, cells were scraped into a tube containing 20 ml of R liquid medium. After 1.5 d, the top 5 ml of the medium was moved to a new tube. The medium was transferred once every 3 d until swimmers were observed. *ida3; oda2* swimmers were visually scored for motility rescue and were analyzed by immunoblot for rescue of the intermediate chains IC140/IC138 as a marker for I1 dynein assembly in the axoneme. Sanger sequencing confirmed the intragenic reversion within *ida3* of the *ida3; oda2* cells exhibiting a rescue phenotype (Supplemental Figure S2, Table III).

Cloning of *IDA3* and transformation and rescue of *ida3* mutants

All cloning and tagging of *IDA3* was completed at the custom cloning core facility at Emory University. Briefly, the *IDA3* gene (~4.2 kB) was PCR-amplified from the BAC (4E5) clone containing the Cre03.g205000 gene. *Chlamydomonas* codon–optimized p3xHA (Silflow *et al.*, 2001) or NeonGreen (Craft *et al.*, 2015; Harris *et al.*, 2016) were inserted into either the N-terminus or C-terminus of IDA3 or embedded within the first or second exon of the *IDA3* gene (Supplemental Figure S2, Table II). All *IDA3*-tagged constructs were inserted into the PUCBM20 vector containing a *Chlamydomonas* Hygromycin B selection marker (pHyg3) (Berthold *et al.*, 2002). The resulting constructs were transformed into the *ida3* mutant by electroporation and placed on TAP+Hygromycin plates (final concentration at 10 µg/ml) for selection of single colonies expressing Hygromycin resistance. Surviving colonies were visually scored for motility rescue of wild-type speed and isolated axonemes from each colony were analyzed by immunoblot for rescue of IC140/IC138 as a marker of I1 dynein assembly in the axoneme.

Preparation of matrix fractions

C. reinhardtii cells grown on constant light in L medium were collected by centrifugation and resuspended in chilled deciliation buffer (10 mM Tris, pH 7.5, 5% sucrose, 1 mM $CaCl_2$) and kept on ice. *C. reinhardtii* cells were deciliated by pH shock (Alford *et al.*, 2013; Hunter *et al.*, 2016). Cells were resuspended in room temperature L medium and aerated for 35 min at room temperature on constant light to regenerate cilia to approximately half length (Hunter *et al.*, 2016). Regeneration of cilia was observed by phase contrast microscopy. Cells were collected by centrifugation

(3000 rpm for 5 min) and again resuspended in chilled deciliation buffer. A second deciliation was induced on ice by pH shock and flagella were collected by subsequent centrifugation.

To isolate the matrix fraction, cilia were resuspended in HMDE + 25 mM NaCl (10 mM HEPES, 5 mM $MgSO_4$, 1 mM DTT [dithiothreitol], 0.5 mM EDTA, 25 mM NaCl, protease inhibitors, pH 7.4). EDTA was omitted from HMDE + 25 mM NaCl buffer for all SNAP pull-down experiments. Cilia were flash frozen in liquid nitrogen and thawed at room temperature prior to centrifugation to remove remaining axonemes and membranes from the matrix fraction (Cole *et al.*, 1998; Lucker *et al.*, 2005; Pazour *et al.*, 2005; Craige et al., 2013). Matrix fractions were either stored at 4°C prior to use in immunoprecipitation/pull-down analyses or denatured with Laemmli sample buffer for immunoblot analysis. For matrix fractions of full-length cilia, the regeneration step was omitted, and cilia were isolated by pH shock and centrifugation prior to matrix isolation through identical freeze–thaw methods.

Antibodies and immunoblot analyses

SDS–PAGE and immunoblotting were performed using standard procedures. Primary antibodies used in this study include mouse monoclonal antibody (mAb) against HA (Clone 12CA5; Roche, Mannheim, Germany) and IFT57 (Cole *et al.*, 1998; Hou *et al.*, 2007). Rabbit polyclonal antibodies include IC140 (Yang and Sale, 1998), IC138 (Hendrickson *et al.*, 2004), and RSP3 (Wirschell *et al.*, 2008). The secondary antibodies goat anti-mouse (#1706516) and goat anti-rabbit (#1706515) were purchased from Biorad.

Isolation of axonemes

Cells were grown to mid–log phase and deciliated either by pH shock (Lefebvre, 1995; Hunter *et al.*, 2016) or by treating the cells with dibucaine (Witman, 1986). After centrifugation to separate cilia from cell bodies, the cilia were demembranated by final 1% Nonidet P-40 (EMD Millipore, Darmstadt, Germany) in HMDE +25 mM NaCl (10 mM HEPES, 5 mM $MgSO_4$, 1 mM DTT, 0.5 mM EDTA, 25 mM NaCl, protease inhibitors, pH 7.4). Post centrifugation, the axoneme pellet was resuspended in HMDE +25 mM NaCl + protease inhibitors and denatured for immunoblot analyses in Laemmli sample buffer at a final concentration of 1 mg/ml.

Isolation of cytoplasmic extracts

Glass beads were used to lyse cells cultured for 3 d (Ahmed *et al.*, 2008). Broken cells were clarified by centrifugation at 10,000 rpm in a Sorval SA600 rotor for 10 min. The supernatant was then further clarified at 22,500 rpm for 2 h (Type-40 fixed angle rotor, Beckman Coulter). Clarified supernatant was collected and denatured with Laemmli sample buffer for immunoblot analysis.

Electron microscopy

Conventional electron microscopy was performed on axonemes isolated from CC125, *ida3,* and *ida3; IDA3::HA* cells as previously described (Kamiya *et al.*, 1991).

Cryo-electron tomography

Axoneme preparation for cryo–ET. Strains of *C. reinhardtii* were first grown on solid agar plates made with Tris-acetate-phosphate (TAP) medium for 5–7 d (Harris, 2009), and then a small amount of cells were transferred to liquid TAP growth medium for 3–4 d culturing under 12:12 h light:dark regime and flask shaking with the speed of 120 rpm. Cells were harvested by centrifugation (2200 rpm) and resuspended in 10 mM HEPES buffer, pH 7.4 (1 mM $SrCl_2$, 4% sucrose, and 1 mM DTT). Cilia were isolated using the pH shock method (Witman *et al.*, 1972); in brief, cell pellets were resuspended in HEPES buffer (4% sucrose, 1 mM $SrCl_2$, 10 mM HEPES, 1% DTT, pH 7.4) and the pH lowered to 4.5 by adding 0.5 M acetate acid. After 80 s, the pH value was brought back to 7.4 by adding 1 M KOH. After detachment of the cilia from the cell bodies the following solution was added to the buffer: 5 mM $MgSO_4$, 1 mM EGTA (ethylene glycol-bis(β-amino ethyl ether)-*N*,*N*,*N*′*N*′-tetraacedtic acid), 0.1 mM EDTA, and 100 µl protease inhibitor cocktails (Sigma-Aldrich). Cilia were washed two times over a 20% sucrose cushion and then demembranated with 0.1% IGEPAL CA-630 (Sigma-Aldrich). Axonemes were collected by centrifugation at 10,000 × *g* for 10 min and resuspended in HMEEK buffer (30 mM HEPES, 25 mM KCl, 5 mM $MgSO_4$, 0.1 mM EDTA, and 0.2 mM EGTA). Cilia isolation and all steps thereafter were performed on ice or at 4°C.

Cryo–sample preparation, cryo–electron tomography, and image processing. Freshly prepared axonemes were plunge-frozen on glow discharged (for 30 s at –35 mA) grids with holey carbon film (copper; R2/2; 200 meshes; Quantifoil Micro Tools GmbH, Jena, Germany) using a homemade plunge freezer to achieve sample vitrification, as previously described (Heuser *et al.*, 2009). In brief, 3 µl of axoneme sample was applied to the grid and gently mixed with 1 µl of 10× concentrated 10-nm colloidal gold solution. The gold particles were precoated with 5% (wt/vol) BSA (bovine serum albumen) solution to help prevent their aggregation (Iancu *et al.*, 2006). Grids were blotted with Whatman filter paper from the back for 1.5–2.5 s and rapidly plunged into liquid ethane. Sample grids were stored in liquid nitrogen until used.

Vitrified axonemes were imaged on a Tecnai F30 transmission electron microscope (Thermo-Fisher/FEI) operated at 300 kV. Tilt series (from –60° to 60°; 1.5°–2.5° tilting increments) were recorded with a 2*k* × 2*k* charge-coupled device camera (Gatan, Pleasanton, CA) after energy filtering (Gatan) in zero-loss mode (20 eV slit width). Using the low dose mode in the microscope control and data acquisition software SerialEM (Mastronarde, 2005) the total electron dose per tilt series was limited to ~100 e/Å^2 to avoid radiation damage. A magnification of 13,500 (pixel size of 1 nm) and a defocus of –8 µm were used for imaging.

For image processing, the tilt series images were aligned using the 10 nm gold as fiducial markers. Both alignment and tomogram reconstruction by weighted back-projection were performed using the IMOD software package (Kremer *et al.*, 1996). The axonemal 96 nm repeats were picked from the raw tomograms, aligned and subtomogram averaged using the PEET software (Nicastro *et al.*, 2006). Three-dimensional (3D) visualization of the averaged structures by isosurface rendering was performed with UCSF Chimera package (Pettersen *et al.*, 2004). Automated classification analyses of the I1 inner dynein arm were carried out with a PCA (principal component analysis) clustering approach (Heumann *et al.*, 2011).

TIRF microscopy

For TIRF imaging, we used an Eclipse Ti-U microscope (Nikon) equipped with a 60× NA1.49 TIRF objective and through-the-objective TIRF illumination provided by a 40-mW 488-nm diode laser (Spectraphysics) (Lechtreck, 2013). Excitation and emission were filtered using the Nikon GFP/mCherry TIRF filter and the emission was separated using an image splitting device (Photometrics DualView2 with filter cube 11-EM). Observation chambers for live cell imaging were assembled by inverting a 22 × 22 mm No. 1.5 cover glass with ~10 µl of 5 mM HEPES, pH 7.3, 6.25 mM EGTA onto an equal volume of cells in M medium on a 24 × 60 mm No. 1.5 cover

glass. Images were recorded at 10 fps using an iXON3 (Andor) and the NIS-Elements Advanced Research software (Nikon). FIJI (ImageJ plug-in bundle; National Institutes of Health) was used to generate kymograms (Lechtreck, 2016). Individual frames were copied into Photoshop (Adobe) and adjusted for contrast and brightness; figures were assembled in Illustrator (CS6 version 16.0.3, Adobe). To generate videos, stacks were saved in avi format. For photobleaching of the entire cilia, the intensity of the 488-nm laser was increased to 10% or more for 4–12 s (Wingfield *et al.*, 2017).

To examine regenerating cilia, cells were deflagellated by a pH shock, washed into fresh M medium, and incubated with agitation in bright light. To delay regeneration, cells were stored on ice until needed. For long–short experiments, cells were passaged four to six times through a 26G × 1/2 needle using a 1-ml syringe. This treatment resulted in a small percentage (~1%) of long-zero cells that were imaged using TIRF microscopy after flagellar regeneration was allowed for ~10–20 min.

Immunoprecipitation of IDA3::HA

All immunoprecipitation experiments were performed in matrix fractions isolated from regenerating cilia (as described above). To perform HA immunoprecipitation analyses, matrix fractions were isolated from regenerating cilia of *ida3* (CC-2688) and *ida3; IDA3::HA* strains. Immunoprecipitation (IP) buffer consists of 10 mM HEPES (pH 7.4), 5 mM $MgSO_4$, 1 mM DTT, 0.1 mM EDTA, 25 mM KCl, 75 mM NaCl, and 0.05% Triton X-100. Part of each matrix fraction was denatured with Laemmli sample buffer for analysis of input by immunoblotting. The rest of the matrix fraction was preincubated with protein A agarose beads (Invitrogen) for 1 h at 4°C with slight agitation to preclear it. Prior to immunoprecipitation, 3F10-crosslinked beads (Roche) were blocked with 3% BSA in IP buffer by rocking for 1 h at 4°C. Precleared matrix fractions and preblocked 3F10-crosslinked beads were collected by centrifugation and combined for immunoprecipitation overnight at 4°C with slight agitation. Immunoprecipitates were washed with IP buffer the next day and denatured with 2× Laemmli sample buffer. Input samples and immunoprecipitates were resolved by SDS–PAGE and analyzed by immunoblotting.

SNAP affinity purification

Matrix fractions were prepared by freeze–thaw, stored at 4°C, and supplemented with 0.5% Triton X-100 prior to use. For affinity purification, we used a modified protocol from Zlatic *et al.* (Zlatic *et al.*, 2013). SNAP magnetic beads (Cat. No. S9145S; New England Biolabs) were prepared as follows: for each strain, 40 µl of the SNAP magnetic beads were spun down at room temperature using a bench-top minicentrifuge at top speed (14,000 × *g*) for 1 min. The clarified supernatant was removed and the beads were incubated overnight in an end-over-end rocker at 4°C in a buffer containing 3% BSA, 10 mM HEPES, 5 mM $MgSO_4$, 1 mM DTT, 25 mM NaCl, and protease inhibitors at pH 7.4. Fresh DTT and protease inhibitors were added to the buffer solution every day prior to use. The next day, the beads were washed twice in a buffer containing 10 mM HEPES, 5 mM $MgSO_4$, 1 mM DTT, 0.5 mM EDTA, 25 mM NaCl, 0.5% Triton X-100, and protease inhibitors at pH 7.4 using the magnetic holder. Matrix fractions were then added to the SNAP beads and the mixture was incubated at 4°C in an end-over-end rotor overnight. The magnetic beads were then washed six times in a buffer containing 10 mM HEPES, 5 mM $MgSO_4$, 1 mM DTT, 0.5 mM EDTA, 25 mM NaCl, 0.5% Triton X-100, and protease inhibitors at pH 7.4. The beads were then resuspended in 2× Laemmli sample buffer and denatured at 95°C for 5 min for immunoblot analysis.

Analysis of processive IDA3 movement in *ida7; ida3; IDA3::NG*

TIRF microscopy was used to visualize IDA3 transport in regenerating *ida3; IDA3::NG* and *ida7; ida3; IDA3::NG* cells. Both cell types were imaged when cilia were approximately the same length (roughly 7–9 µm). Subsequent kymograms were generated. The length of the cilium and the length of anterograde IFT tracks were measured using ImageJ Software (National Institutes of Health). Any kymograms in which the tip of the cilium could not be clearly distinguished were excluded from the analysis. The ratio of anterograde IFT track length to cilium length was then determined.

Statistical analysis

To determine whether a statistical difference between anterograde IFT (or retrograde transport) vs. diffusion of IDA3 exists, a two-tailed binomial test was performed in Graphpad software (www.graphpad.com) as described before (Lechtreck, 2013). To determine whether a statistical difference exists between IDA3 IFT transport in the presence or absence of I1, a two-tailed unpaired *t* test was performed in Graphpad software. The graphs were drawn with Adobe Illustrator and Excel.

ACKNOWLEDGMENTS

This research was supported by funding from the National Institutes of Health (NIH) (W.S.S. and M.W., GM051173; K.L., GM1100413; D.N., GM083122; and S.K.D., HL128370) and the Children's Discovery Institute, PD-II-2014-379 to S.K.D. E.L.H. was supported by a Greater Southeast Affiliate Pre-doctoral Fellowship from the American Heart Association (10PRE353007) and by a Biochemistry, Cell, and Molecular Biology (BCMB) Training Grant at Emory University (NIH T32 GM008367). A.G. was supported in part by an Emory University Catalyst Grant. This study was also supported in part by the Emory Integrated Genomics Core (EIGC), which is subsidized by the Emory University School of Medicine and is one of the Emory Integrated Core Facilities. R.Y. was the recipient of a Postdoctoral Fellowship for Research Abroad from the Japan Society for the Promotion of Science (JSPS). Additional support for sequencing was provided by the National Center for Advancing Translational Sciences of the National Institutes of Health under Award No. UL1TR000454. We are grateful to T. Oda (Department of Anatomy and Structural Biology, Graduate School of Medical Science, University of Yamanashi) for the gift of the *ida7; IC140::GFP* cells. The content is solely the responsibility of the authors and does not necessarily reflect the official views of the National Institutes of Health.

REFERENCES

Ahmed NT, Gao C, Lucker BF, Cole DG, Mitchell DR (2008). ODA16 aids axonemal outer row dynein assembly through an interaction with the intraflagellar transport machinery. J Cell Biol 183, 313–322.

Alford LM, Mattheyses AL, Hunter EL, Lin H, Dutcher SK, Sale WS (2013). The *Chlamydomonas* mutant pf27 reveals novel features of ciliary radial spoke assembly. Cytoskeleton (Hoboken) 70, 804–818.

Awata J, Song K, Lin J, King SM, Sanderson MJ, Nicastro D, Witman GB (2015). DRC3 connects the N-DRC to dynein g to regulate flagellar waveform. Mol Biol Cell 26, 2788–2800.

Berthold P, Schmitt R, Mages W (2002). An engineered *Streptomyces hygroscopicus* aph 7" gene mediates dominant resistance against hygromycin B in *Chlamydomonas reinhardtii*. Protist 153, 401–412.

Bhogaraju S, Weber K, Engel BD, Lechtreck KF, Lorentzen E (2014). Getting tubulin to the tip of the cilium: one IFT train, many different tubulin cargo-binding sites? Bioessays 36, 463–467.

Brown JM, Mosley M, Montes-Berrueta D, Hou Y, Yang F, Scarbrough C, Witman GB, Wirschell M (2017). Characterization of a new oda3 allele, oda3–6, defective in assembly of the outer dynein arm-docking complex in *Chlamydomonas reinhardtii*. PLoS One 12, e0173842.
Chien A, Shih SM, Bower R, Tritschler D, Porter ME, Yildiz A (2017). Dynamics of the IFT machinery at the ciliary tip. Elife 6, e28606.
Cole DG, Diener DR, Himelblau AL, Beech PL, Fuster JC, Rosenbaum JL (1998). *Chlamydomonas* kinesin-II-dependent intraflagellar transport (IFT): IFT particles contain proteins required for ciliary assembly in *Caenorhabditis elegans* sensory neurons. J Cell Biol 141, 993–1008.
Craft JM, Harris JA, Hyman S, Kner P, Lechtreck KF (2015). Tubulin transport by IFT is upregulated during ciliary growth by a cilium-autonomous mechanism. J Cell Biol 208, 223–237.
Craige B, Brown JM, Witman GB (2013). Isolation of *Chlamydomonas* flagella. Curr Protoc Cell Biol Chapter 3, Unit 3 41 41–49.
Desai PB, Freshour JR, Mitchell DR (2015). *Chlamydomonas* axonemal dynein assembly locus ODA8 encodes a conserved flagellar protein needed for cytoplasmic maturation of outer dynein arm complexes. Cytoskeleton (Hoboken) 72, 16–28.
Dutcher SK (1995). Mating and tetrad analysis in *Chlamydomonas reinhardtii*. Methods Cell Biol 47, 531–540.
Harris EH (2009). The *Chlamydomonas* Sourcebook: Introduction to *Chlamydomonas* and Its Laboratory Use, Oxford, UK: Academic Press.
Harris JA, Liu Y, Yang P, Kner P, Lechtreck KF (2016). Single-particle imaging reveals intraflagellar transport-independent transport and accumulation of EB1 in *Chlamydomonas* flagella. Mol Biol Cell 27, 295–307.
Hendrickson TW, Perrone CA, Griffin P, Wuichet K, Mueller J, Yang P, Porter ME, Sale WS (2004). IC138 is a WD-repeat dynein intermediate chain required for light chain assembly and regulation of flagellar bending. Mol Biol Cell 15, 5431–5442.
Heumann JM, Hoenger A, Mastronarde DN (2011). Clustering and variance maps for cryo-electron tomography using wedge-masked differences. J Struct Biol 175, 288–299.
Heuser T, Barber CF, Lin J, Krell J, Rebesco M, Porter ME, Nicastro D (2012). Cryoelectron tomography reveals doublet-specific structures and unique interactions in the I1 dynein. Proc Natl Acad Sci USA 109, E2067–E2076.
Heuser T, Raytchev M, Krell J, Porter ME, Nicastro D (2009). The dynein regulatory complex is the nexin link and a major regulatory node in cilia and flagella. J Cell Biol 187, 921–933.
Horani A, Ferkol TW, Dutcher SK, Brody SL (2016). Genetics and biology of primary ciliary dyskinesia. Paediatr Respir Rev 18, 18–24.
Hou Y, Qin H, Follit JA, Pazour GJ, Rosenbaum JL, Witman GB (2007). Functional analysis of an individual IFT protein: IFT46 is required for transport of outer dynein arms into flagella. J Cell Biol 176, 653–665.
Hou Y, Witman GB (2017). The N-terminus of IFT46 mediates intraflagellar transport of outer arm dynein and its cargo-adaptor ODA16. Mol Biol Cell 28, 2420–2433.
Hunter EL, Sale WS, Alford LM (2016). Analysis of axonemal assembly during ciliary regeneration in *Chlamydomonas*. Methods Mol Biol 1454, 237–243.
Iancu CV, Tivol WF, Schooler JB, Dias DP, Henderson GP, Murphy GE, Wright ER, Li Z, Yu Z, Briegel A, *et al*. (2006). Electron cryotomography sample preparation using the Vitrobot. Nat Protoc 1, 2813–2819.
Iomini C, Till JE, Dutcher SK (2009). Genetic and phenotypic analysis of flagellar assembly mutants in *Chlamydomonas reinhardtii*. Methods Cell Biol 93, 121–143.
Ishikawa H, Marshall WF (2017). Testing the time-of-flight model for flagellar length sensing. Mol Biol Cell 28, 3447–3456.
Ishikawa T (2012). Organization of dyneins in the axoneme. In: Dyneins: Structure, Biology and Disease, ed. SM King, London, UK: Elsevier Academic Press, 245–271.
Kamiya R, Kurimoto E, Muto E (1991). Two types of *Chlamydomonas* flagellar mutants missing different components of inner-arm dynein. J Cell Biol 112, 441–447.
Kamiya R, Yagi T (2014). Functional diversity of axonemal dyneins as assessed by in vitro and in vivo motility assays of *Chlamydomonas* mutants. Zoolog Sci 31, 633–644.
Kindle KL (1990). High-frequency nuclear transformation of *Chlamydomonas reinhardtii*. Proc Natl Acad Sci USA 87, 1228–1232.
King SM (2016). Axonemal dynein arms. Cold Spring Harb Perspect Biol 8.
Knowles MR, Zariwala M, Leigh M (2016). Primary ciliary dyskinesia. Clin Chest Med 37, 449–461.
Kobayashi D, Takeda H (2012). Ciliary motility: the components and cytoplasmic preassembly mechanisms of the axonemal dyneins. Differentiation 83, S23–S29.
Kremer JR, Mastronarde DN, McIntosh JR (1996). Computer visualization of three-dimensional image data using IMOD. J Struct Biol 116, 71–76.
Kubo T, Brown JM, Bellve K, Craige B, Craft JM, Fogarty K, Lechtreck KF, Witman GB (2016). Together, the IFT81 and IFT74 N-termini form the main module for intraflagellar transport of tubulin. J Cell Sci 129, 2106–2119.
Lechtreck KF (2013). In vivo imaging of IFT in *Chlamydomonas* flagella. Methods Enzymol 524, 265–284.
Lechtreck KF (2015). IFT-cargo interactions and protein transport in cilia. Trends Biochem Sci 40, 765–778.
Lechtreck KF (2016). Methods for studying movement of molecules within cilia. Methods Mol Biol 1454, 83–96.
Lechtreck KF, Van De Weghe JC, Harris JA, Liu P (2017). Protein transport in growing and steady-state cilia. Traffic 18, 277–286.
Lefebvre PA (1995). Flagellar amputation and regeneration in *Chlamydomonas*. Methods Cell Biol 47, 3–7.
Lin H, Dutcher SK (2015). Genetic and genomic approaches to identify genes involved in flagellar assembly in *Chlamydomonas reinhardtii*. Methods Cell Biol 127, 349–386.
Lin H, Miller ML, Granas DM, Dutcher SK (2013). Whole genome sequencing identifies a deletion in protein phosphatase 2A that affects its stability and localization in *Chlamydomonas reinhardtii*. PLoS Genet 9, e1003841.
Lucker BF, Behal RH, Qin H, Siron LC, Taggart WD, Rosenbaum JL, Cole DG (2005). Characterization of the intraflagellar transport complex B core: direct interaction of the IFT81 and IFT74/72 subunits. J Biol Chem 280, 27688–27696.
Mastronarde DN (2005). Automated electron microscope tomography using robust prediction of specimen movements. J Struct Biol 152, 36–51.
Nicastro D, Schwartz C, Pierson J, Gaudette R, Porter ME, McIntosh JR (2006). The molecular architecture of axonemes revealed by cryoelectron tomography. Science 313, 944–948.
Oda T, Yanagisawa H, Kikkawa M (2015). Detailed structural and biochemical characterization of the nexin-dynein regulatory complex. Mol Biol Cell 26, 294–304.
Ostrowski LE, Dutcher SK, Lo CW (2011). Cilia and models for studying structure and function. Proc Am Thorac Soc 8, 423–429.
Owa M, Furuta A, Usukura J, Arisaka F, King SM, Witman GB, Kamiya R, Wakabayashi K (2014). Cooperative binding of the outer arm-docking complex underlies the regular arrangement of outer arm dynein in the axoneme. Proc Natl Acad Sci USA 111, 9461–9466.
Pasquale SM, Goodenough UW (1987). Cyclic AMP functions as a primary sexual signal in gametes of *Chlamydomonas reinhardtii*. J Cell Biol 105, 2279–2292.
Pazour GJ, Agrin N, Leszyk J, Witman GB (2005). Proteomic analysis of a eukaryotic cilium. J Cell Biol 170, 103–113.
Perrone CA, Yang P, O'Toole E, Sale WS, Porter ME (1998). The *Chlamydomonas* IDA7 locus encodes a 140-kDa dynein intermediate chain required to assemble the I1 inner arm complex. Mol Biol Cell 9, 3351–3365.
Pettersen EF, Goddard TD, Huang CC, Couch GS, Greenblatt DM, Meng EC, Ferrin TE (2004). UCSF Chimera–a visualization system for exploratory research and analysis. J Comput Chem 25, 1605–1612.
Redwine WB, DeSantis ME, Hollyer I, Htet ZM, Tran PT, Swanson SK, Florens L, Washburn MP, Reck-Peterson SL (2017). The human cytoplasmic dynein interactome reveals novel activators of motility. Elife 6, e28257.
Silflow CD, LaVoie M, Tam LW, Tousey S, Sanders M, Wu W, Borodovsky M, Lefebvre PA (2001). The Vfl1 protein in *Chlamydomonas* localizes in a rotationally asymmetric pattern at the distal ends of the basal bodies. J Cell Biol 153, 63–74.
Sizova IA, Lapina TV, Frolova ON, Alexandrova NN, Akopiants KE, Danilenko VN (1996). Stable nuclear transformation of *Chlamydomonas reinhardtii* with a Streptomyces rimosus gene as the selective marker. Gene 181, 13–18.
Stepanek L, Pigino G (2016). Microtubule doublets are double-track railways for intraflagellar transport trains. Science 352, 721–724.
Taschner M, Lorentzen E (2016). The intraflagellar transport machinery. Cold Spring Harb Perspect Biol 8, a028092.
Taschner M, Mourao A, Awasthi M, Basquin J, Lorentzen E (2017). Structural basis of outer dynein arm intraflagellar transport by the transport adaptor protein ODA16 and the intraflagellar transport protein IFT46. J Biol Chem 292, 7462–7473.
Taschner M, Weber K, Mourao A, Vetter M, Awasthi M, Stiegler M, Bhogaraju S, Lorentzen E (2016). Intraflagellar transport proteins 172, 80, 57, 54, 38, and 20 form a stable tubulin-binding IFT-B2 complex. EMBO J 35, 773–790.

Viswanadha R, Hunter EL, Yamamoto R, Wirschell M, Alford LM, Dutcher SK, Sale WS (2014). The ciliary inner dynein arm, I1 dynein, is assembled in the cytoplasm and transported by IFT before axonemal docking. Cytoskeleton (Hoboken) 71, 573–586.

Viswanadha R, Sale WS, Porter ME (2017). Ciliary motility: regulation of axonemal dynein motors. Cold Spring Harb Perspect Biol 9, a018325.

Wingfield JL, Mengoni I, Bomberger H, Jiang YY, Walsh JD, Brown JM, Picariello T, Cochran DA, Zhu B, Pan J, *et al.* (2017). IFT trains in different stages of assembly queue at the ciliary base for consecutive release into the cilium. Elife 6, e26609.

Wirschell M, Hendrickson T, Sale WS (2007). Keeping an eye on I1: I1 dynein as a model for flagellar dynein assembly and regulation. Cell Motil Cytoskeleton 64, 569–579.

Wirschell M, Zhao F, Yang C, Yang P, Diener D, Gaillard A, Rosenbaum JL, Sale WS (2008). Building a radial spoke: flagellar radial spoke protein 3 (RSP3) is a dimer. Cell Motil Cytoskeleton 65, 238–248.

Witman GB (1986). Isolation of *Chlamydomonas* flagella and flagellar axonemes. Method Enzymol 134, 280–290.

Witman GB, Carlson K, Berliner J, Rosenbaum JL (1972). *Chlamydomonas* flagella. I. Isolation and electrophoretic analysis of microtubules, matrix, membranes, and mastigonemes. J Cell Biol 54, 507–539.

Wren KN, Craft JM, Tritschler D, Schauer A, Patel DK, Smith EF, Porter ME, Kner P, Lechtreck KF (2013). A differential cargo-loading model of ciliary length regulation by IFT. Curr Biol 23, 2463–2471.

Yang P, Sale WS (1998). The Mr 140,000 intermediate chain of *Chlamydomonas* flagellar inner arm dynein is a WD-repeat protein implicated in dynein arm anchoring. Mol Biol Cell 9, 3335–3349.

Zlatic SA, Grossniklaus EJ, Ryder PV, Salazar G, Mattheyses AL, Peden AA, Faundez V (2013). Chemical-genetic disruption of clathrin function spares adaptor complex 3-dependent endosome vesicle biogenesis. Mol Biol Cell 24, 2378–2388.